Available online at www.sciencedirect.com
SCIENCE DIRECT®
Bioelectrochemistry 68 (2006) 181 – 190
Bioelectrochemistry
www.elsevier.com/locate/bioelechem

Model of a confined spherical cell in uniform and heterogeneous applied electric fields

T.R. Gowrishankar, Donald A. Stewart, James C. Weaver *

Harvard-M.I.T. Division of Health Sciences and Technology, Massachusetts Institute of Technology, 16-319, 77 Massachusetts Avenue, Cambridge, MA 02139, USA

Received 7 March 2005; received in revised form 20 July 2005; accepted 30 July 2005
Available online 17 October 2005

Abstract

Cells exposed to electric fields are often confined to a small volume within a solid tissue or within or near a device. Here we report on an approach to describing the frequency and time domain electrical responses of a spatially confined spherical cell by using a transport lattice system model. Two cases are considered: (1) a uniform applied field created by parallel plane electrodes, and (2) a heterogeneous applied field created by a planar electrode and a sharp microelectrode. Here fixed conductivities and dielectric permittivities of the extra- and intracellular media and of the membrane are used to create local transport models that are interconnected to create the system model. Consistent with traditional analytical solutions for spherical cells in an electrolyte of infinite extent, in the frequency domain the field amplification, $G_m(f)$ is large at low frequencies, $f<1$ MHz. $G_m(f)$ gradually decreases above 1 MHz and reaches a lower plateau at about 300 MHz, with the cell becoming almost "electrically invisible". In the time domain the application of a field pulse can result in altered localized transmembrane voltage changes due to a single microelectrode. The transport lattice approach provides modular, multiscale modeling capability that here ranges from cell membranes (5 nm scale) to the cell confinement volume (~40 μm scale).
© 2005 Elsevier B.V. All rights reserved.

Keywords: Three dimensional cell model; Transport lattice; Electric field; Spherical cell; Cell membrane; Confined cell; Microelectrode

1. Introduction

Theory and modeling related to biological cells and tissues exposed to electric fields is of long-standing interest [1–8]. Although heating is unavoidable, the temperature rise due to Joule heating of the aqueous extracellular medium can be small, and the main effects are due to electrostatic interactions. In this case the molecular change directly attributable to heating during a field exposure is smaller than the cumulative molecular change due to biophysical mechanisms based on electrostatic interactions. Electrostatic effects can be designated as nonthermal, because the predominant molecular change is not caused by a temperature rise. Moreover, to create an effect which persists after the exposure there should be a lasting change, which generally involves a field-induced chemical change [9].

Examples of these effects are net transport of ions controlled by voltage-gated channels at moderate field strengths [6,8] and weak fields [1,9–12], enzyme electroconformational coupling [13,14], electroporative release of molecules [15–18] or uptake of molecules [7,19–27], and electro-insertion of macromolecules into cell membranes [28,29]. Intracellular effects may involve both the cell's outer plasma membrane and internal organelle membranes [30–36]. At the tissue level, effects include both beneficial electroporation for drug delivery [37–39,7] and damaging electroporation that is the basis for nonthermal electrical injury [40,41].

Electrostatic interactions of cells with an applied electric field, $\vec{E}_{app}$ result in spatially distributed, field-altered transmembrane voltage, U_m induced across the cell membrane. Large voltage concentration at the membrane occurs unless the extracellular medium has very low conductivity or the frequency content of the applied field is larger than about 300 MHz [42,43]. The spatial distribution of U_m depends on the cell size and shape, orientation with respect to the applied field, and the conductivities and permittivities of the membrane, cytoplasm, and both the extra- and intracellular media. The response electric field, $\vec{E}_{res}$ and U_m behavior also depend on the composition and proximity of other objects such as

* Corresponding author. Tel.: +1 617 253 4194; fax: +1 617 253 2514.
E-mail addresses: tgowrish@mit.edu (T.R. Gowrishankar), stewy@mit.edu (D.A. Stewart), jcw@mit.edu (J.C. Weaver).

1567-5394/$ - see front matter © 2005 Elsevier B.V. All rights reserved.
doi:10.1016/j.bioelechem.2005.07.002

electrically insulating walls of a small container holding one or more cells, and field sources such as planar electrodes or proximal sharp microelectrodes.

The theory of field-induced transmembrane voltage change for a spherical cell was introduced by Fricke [44], and expanded by Pauly and Schwan [45] to include dielectric and conductive properties for both electrolytes and the membrane, but the approximation that the aqueous electrolytes are purely conductive was then often made. A brief review of transmembrane voltage change in isolated cells by uniform applied fields appears in a recent paper on spheroidal cells [46]. Both a polarization model for spheroidal cells [47] and a second-order model [42] account for the dielectric properties of the cytoplasm and the extracellular medium, which become important at high frequencies. Such models show that the membrane field amplification, $G_m(f)$, can be large at low frequencies ($\vec{E}_{res}$ dominated by conductive voltage division), but decreases and then levels off to a high frequency plateau ($\vec{E}_{res}$ dominated by dielectric voltage division) [42,43].

Traditionally modeling has focused on two-dimensional analytic solutions for cylindrical (circular) cells, and in three-dimensions on analytical treatment of spheroidal (including spherical) and ellipsoidal cells [42,44–46,48–53]. Confined spherical cells have also been treated using symmetry-exploiting analysis [54,55]. However, numerical analysis is needed for more complex cell shapes [56,57]. Microelectrode models intrinsically involve heterogeneous fields and are generally based on traditional numerical methods [58,59]. The heterogeneous microelectrode fields are used to stimulate excitable cells and tissues locally [60–62] manipulate cells by dielectrophoresis [63–66], carry out localized electrochemical analysis [67], and to cause localized electroporation and electrofusion of cells [68–70]. The small size and sharp boundaries of microelectrodes create highly inhomogeneous fields even without cells or tissue present. It is therefore of interest to consider models that can be used for spatially confined cells, and also cells close to microelectrodes, particularly if such models have the prospect of being extended to include nonlinear interaction mechanisms such as the resting potential [43], membrane electroporation [71], and molecular change through intracellular accumulation by rectification of ionic fluxes [72]. Indeed, some previous models have incorporated both the resting potential and a nonlinear, hysteretic model for membrane electroporation in the case of a spherical cell exposed to a spatially uniform electric field pulse created by infinitely distant electrodes [73,74]. Here we explore further a transport lattice approach.

2. Methods

2.1. Transport lattice system model construction

Construction of a transport lattice allows multiple passive and active local models to be interconnected, to create system models with increasingly realistic features [43,71,75–77]. A method has been described [78] where an equivalent circuit model has been used for analyzing chains of gap junction-connected cells using relatively simple circuits. Others have considered RC submodels of isolated cells [47], or have used a closely related approach that exploits spherical membrane symmetry [55,79].

As described elsewhere [43] we construct a system model that contains aqueous electrolytes, the cell's outer (plasma) membrane and two electrodes by a creating a transport lattice with elementary regions that contain intranodal charge transport models (Fig. 1). Sites of cell membranes and electrodes are prescribed by mathematical equations, which are mapped onto a coordinate system to define elementary regions for assignment of local transport models. Ideal electrodes providing the applied field, $\vec{E}_{app}$ are created by assigning their nodes a common potential. The response field $\vec{E}_{res}$ originating from the presence of one or more cells reflects the redistribution of current and fields within the system, which is often dominated by cell membranes and other structures with large resistivities.

Extracellular and intracellular electrolytes are represented by four identical transport models, M_{e1} and M_{e2}, respectively, connected to a central node (Fig. 1). Each of these local models is represented by a resistance (R_{e1} or R_{e2}) in parallel with a capacitance (C_{e1} or C_{e2}). For a given lattice spacing, ℓ, an elementary volume (ℓ^3) of electrolyte (e_1 or e_2) has $R_e=\rho_e/\ell$ (resistivity ρ_e) and $C_e=\epsilon_e\epsilon_0\ell$ (dielectric constant ϵ_e).

The local model for a membrane interfacing with two electrolytes, $M_{e1+m+e2}$, has submodels for charge transport within: (1) electrolyte 1 contacting one side of the membrane, (2) the membrane, and (3) electrolyte 2 contacting the other side of the membrane. For $\ell \gg d_m$ the membrane thickness (5 nm), the electrolytes are approximated by parallel combinations $R_{e1}/2$ and $2C_{e1}$, and $R_{e2}/2$ and $2C_{e2}$ (Fig. 1).

For a uniform $\vec{E}_{app}$ the top and bottom boundaries are ideal planar electrodes. An example of a very heterogeneous $\vec{E}_{app}$ is provided by replacing one planar electrode with a small, discretized tetrahedral electrode that represents a sharp microelectrode. Based on quasi-electrostatic and penetration depth criteria [80], both models are valid from dc to $f\sim 2$ GHz.

2.2. Applied electric field pulse

If no cell were present the electric field in the electrolyte within the system volume would be associated with conduction and displacement currents that recognize both the conductive and dielectric properties, which is the origin of the electrolyte's bulk charge relaxation time, $\tau_e=\rho\epsilon\approx 5\times 10^{-10}$ s (physiologic saline). This passive relaxation is represented by a local model (spatial scale ℓ) that consists of affixed resistance and fixed capacitance in parallel [43]. For physiological saline the dielectric constant is nearly independent of frequency up to ~2 GHz [81]. With this in mind, the applied field is created by assigning idealized electrodes (zero overvoltage) to system model nodes that approximate the electrode surfaces. We consider two electrode pairs: (1) parallel plane electrodes that generate a spatially uniform field, and (2) one microelectrode (approximated by a discretized tetrahedron; Fig. 1) and one plane electrode.

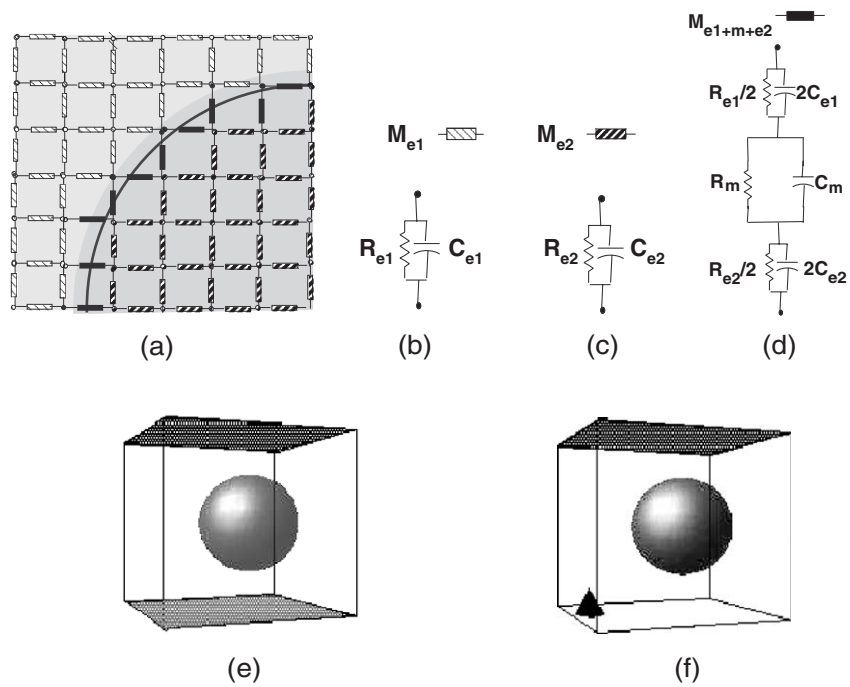

Fig. 1. Illustration of a transport lattice [43]. (a) Small portion of a transport lattice (here 2-D; 7×7 nodes; $6\ell \times 6\ell$ area; 84 local transport models; ℓ = node spacing) with two electrolytes separated by a membrane (curve). (b, c) Electrolyte charge transport models, M_{e1} and M_{e2}. (d) Membrane/two electrolyte interface transport model, $M_{e1+m+e2}$. The cell membrane transport model, M_m is sandwiched between the electrolyte models of half thickness [43]. Two cases described in this paper: (e) homogeneous electric field: a spherical cell is placed between two parallel plate electrodes; (f) heterogeneous electric field: the electric field is generated by a planar electrode and a microelectrode adjacent to the cell. The microelectrode is intentionally offset from the central plane of the system model at $x = -15$ μm and $y = 1$ μm.

The applied field, $\vec{E}_{app}(t)$, is created by applying a time dependent voltage, $V_{app}(t)$ across the electrode pair. In the present analysis we examined the response to a step input with $V_{app} = 1$ V. For a passive membrane U_m at any site is proportional to V_{app}.

2.3. Transport lattice solutions

Both frequency and time domain solutions were obtained by using circuit simulation software based on Kirchhoff's Laws [82,83]. Specifically, we used Berkeley SPICE [83] version 3f5, and MATLAB (Version 7.0.1, MathWorks, Natick, MA) to create SPICE input files. We also used MATLAB to compute equipotentials, transmembrane voltages, and to display results as equipotentials (electric field is perpendicular to the equipotential lines, with closer equipotential spacing corresponding to larger electric fields). We could also retrieve potentials and currents at any node, or for any local model (e.g., M_m to obtain a local response quantity (e.g., U_m as a function of frequency or time. Here we used a single CPU (2.66 GHz) lab-built computer with 4 GB RAM.

2.4. Computational aspects of transport lattice system model

The frequency response (at 101 different frequencies) of the $29 \times 29 \times 29$ spherical cell system model with 26517 variables was computed in 10.5 h. The corresponding transient response (at 67 different time points) was computed in 12 h. significantly, the uniform and heterogeneous models require essentially the same computational power to solve. The system model with extra and intracellular media, cell membrane and electrode map into circuits of similar size and complexity.

3. Results and discussion

As shown in Fig. 1 we created system models by representing a system of electrolytes and cell membranes as a large spatially distributed electrical circuit, a nontraditional way of analyzing spatially distributed charge transport [43]. Other reports [55,79] describe membrane electroporation as a simple conductivity increase rather than using the pore-based asymptotic electroporation model [84–86] and with spatially distributed models [71]. The pore-based model exhibits reversible electrical breakdown, which leads to an approximate voltage plateau during a pulse [87] and also hysteresis due to pore metastability [71]. Equivalent circuit models have also been used to describe cells connected by gap junctions [78], calorimeter devices [88] and heat transport in tissue with heat removal by both heat conduction and blood perfusion [76].

For comparison to analytic results we have solved a transport lattice model for a cell confined to a small volume. Elsewhere we have treated the classic cylindrical cell using both a fixed Cartesian transport lattice and also a meshed lattice that optimizes the model's description of charge transport both normal and parallel to a curved cell membrane [77]. Here we present the results of a coarse model using a Cartesian system model lattice to show key results approximately. There are

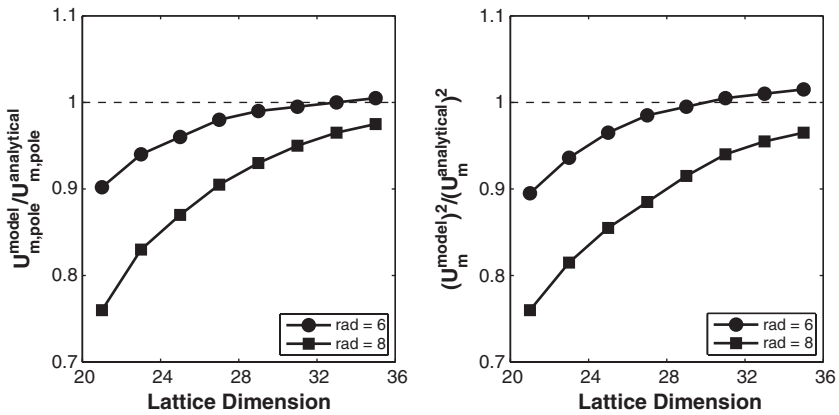

Fig. 2. Comparison of dc U_m from the Cartesian transport lattice model to the analytical spherical model (Eq. (1)). Left: Ratio of model result to analytical value of U_m at the pole as a function of lattice dimension (the number of nodes along any edge of the cubic lattice of the system model). Right: Ratio of model calculation to analytical value of $\overline{U_m^2}$ as a function of lattice dimension of the system model. Here "rad" is the radius of the confined, discretized spherical cell membrane in number of lattice nodes (see Table 1).

three main differences between the lattice and analytical geometries: (1) the system model is based on an approximate representation of the geometry; (2) the membrane is surrounded by a finite amount of extracellular medium, whereas most analytical models assume an infinite extent of extracellular medium; and (3) the transport lattice method with a regular Cartesian coordinate lattice does not include any parallel transport within the membrane (expected to be small because of small thickness and low conductivity of the membrane).

3.1. Uniform applied field

The spherical cell is located in a uniform applied field created by a pair of parallel plane electrodes (Figs. 1–4).

3.1.1. Effect of extracellular volume on $\vec{E}_{res}$ and U_m for a confined cell

If a spherical cell membrane with zero resting potential exists within an extracellular medium of infinite extent and is exposed to a uniform dc applied field then the field-altered transmembrane voltage is

$$U_m = (3/2) r_{cell} E_{app} \cos(\theta) \tag{1}$$

where r_{cell} is the radius of the cell, E_{app} is the applied electric field, and θ is the polar angle with respect to the applied field. This well known equation assumes that the cell membrane thickness is much smaller than r_{cell} and that the membrane conductivity σ_m is much smaller than the conductivities of the extra- and intracellular media, σ_e and σ_i.

Fig. 2 illustrates the effect of a finite extracellular region by comparing the transport lattice model to the analytical solution for a spherical cell in infinite electrolyte (Eq. (1)). The size of the system model was varied from $29 \times 29 \times 29$ to $35 \times 35 \times 35$ and the spherical cell itself ($r_{cell} = 10$ μm) was discretized with 6 and 8 nodes (rad = 6 and 8) spanning the radius of the sphere. As a result, the 8 node case has smaller extracellular region surrounding the cell. Fig. 2 (left) shows the ratio of U_m magnitude at the pole as computed

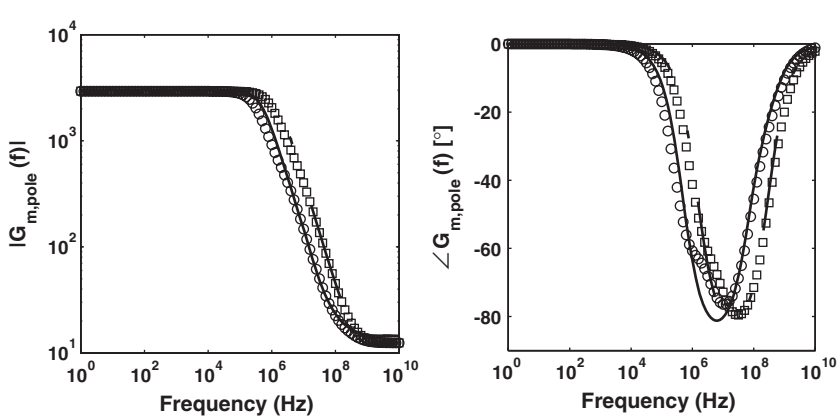

Fig. 3. Frequency dependent field gain magnitude and phase shift at a cell's pole for two electrolyte conditions. The system model of Fig. 1 (e) was used as an analytical solution is available for comparison. The lines are analytical predictions [42] for the case of intra- and extracellular electrolyte being the same (solid lines) and the case of extracellular conductivity a factor of four larger than the intracellular conductivity (dashed lines). The circles (same conductivities) and squares (intracellular conductivity 4× larger than extracellular) are the transport lattice system model predictions for the discretized, confined sphere. Left: gain magnitude. Right: gain phase.

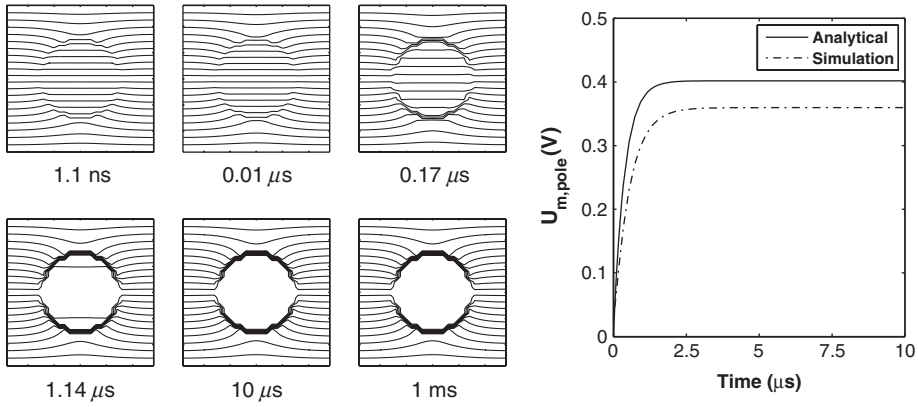

Fig. 4. Step response of a confined spherical cell with a homogeneous applied field. The equipotentials at different time points are shown in the left panel. The corresponding U_m at the pole as a function of time is compared with the analytical solution on the right side. The voltage between the electrodes was increased from 0 to 1 V at $t=0$. U_m reaches the steady-state value in about 1 μs. Prior to that the field penetrates the cell because of its high frequency components. In steady-state the field is excluded from the cell.

by the transport lattice model to that calculated from the analytical expression for different lattice system model sizes. Fig. 2 (right) shows the ratio of membrane-averaged U_m squared obtained from the transport lattice model to that from the analytical expression for different system model sizes. The results show that the model with a larger extracellular region better approximates the analytical case. The $29\times29\times29$ model used in the rest of this paper gives a U_m at the pole that is only 1% less than the analytical solution. The larger discretization error with bigger lattices cause the asymptotic model value to overshoot the analytical value. The behavior is similar in the case of a spherical cell with lesser extracellular medium (cell radius equal to 8 nodes), but, the deviation from the analytical value is larger. U_m at the pole approaches 0.95 of the analytical value with a $35\times35\times35$ lattice. A similar result is obtained for the spatially averaged square of transmembrane voltage (Fig. 2, right) with the overshoot occurring for a lattice dimension of $30\times30\times30$.

At low frequencies or slowly changing pulses the presence of nearby cells or other insulating objects results in a departure from Eq. (1) because current cannot flow through such objects. The altered current density concentration results in local electric field amplification within the electrolyte [43]. If the nearby objects are cells, then current concentration diminishes at high frequencies or for rapidly changing pulses because of displacement current through the membrane. Perturbation of U_m at low frequencies has been investigated by others in cases where system symmetry can be exploited as in the case of spherical cells packed in a cubic arrangement [54,55].

3.1.2. Frequency domain response

Fig. 3 shows the frequency dependent amplitude and phase of membrane field amplification gain ($G_m(f)=U_m(f)/(d_m E_{app}(f))$) [43] at the pole for two different electrolyte conditions. The results are compared with a second-order analytic model [42] for two cases: the conductivities of the cytoplasm and the extracellular medium are same (Table 1); the extracellular medium is four times more conductive than the cytoplasm. $G_{m,pole}(f)$ also agrees with the second order analytic model [42] in both cases, with slight differences arising because of the finite system model region used here.

From dc to ~100 kHz, the large field gain is caused by conduction-dominated voltage division because of the high impedance membrane. With increasing frequency, the displacement current through the membrane begins to increase relative to the conduction current, causing a decline in the field gain. The field gain plateaus at a nonzero value at frequencies above ~300 MHz [43]. The high frequency gain plateau is proportional to the ratio of the dielectric constants of the extracellular medium and the membrane. The transition between the large field gain and the plateau begins around 10 MHz. The transition frequency depends on the ratio of the conductivities of the intracellular and extracellular media (Fig. 3). The high frequency plateau value of the field gain depends on the ratio of the permittivities of the two media. The high frequency plateau in field gain amplitude is reflected in the phase of the field gain raising toward zero beyond the minimum around 300 MHz (Fig. 3).

Table 1
Parameters and their values [42] used in the transport lattice system model

	Parameter	Value
r_{cell}	Cell radius	1×10^{-5} m
	System model dimension	$29\times29\times29$
rad	Cell radius in number of lattice nodes	6 or 8
ℓ	Lattice spacing (rad=6)	1.67×10^{-6} m
ℓ	Lattice spacing (rad=8)	1.25×10^{-6} m
d_m	Membrane thickness	5×10^{-9} m
σ_e	Conductivity of extracellular medium	1.2 S m^{-1}
σ_i	Conductivity of intracellular medium	0.3 S m^{-1}
σ_m	Conductivity of cell membrane	3×10^{-7} S m^{-1}
ϵ_e	Dielectric constant of extracellular medium	72.3
ϵ_i	Dielectric constant of intracellular medium	72.3
ϵ_m	Dielectric constant of cell membrane	5.0

3.1.3. Transient response

The transmembrane voltage (U_m) of a spherical cell of radius r_{cell} exposed to a step input is described by

$$U_m(t) = (3/2)E_{app}r_{cell}\left(1 - e^{-t/\tau_m}\right) \quad (2)$$

where the time constant of the response is

$$\tau_m = \frac{r_{cell}\cdot(\epsilon_m/d_m)}{\dfrac{2\sigma_i\sigma_e}{\sigma_i + 2\sigma_e} + \dfrac{r_{cell}}{d_m}\sigma_m}. \quad (3)$$

In this version of the traditional treatment the dielectric properties of extracellular electrolytes are neglected, i.e., the two media are treated as purely conductive. Because the conductivity of the extracellular and intracellular electrolytes are several orders larger than the conductivity of the membrane and the thickness of the membrane is much smaller than the radius of the cell, the approximate expression agrees to within 0.5% of the full model [77].

Fig. 4 shows the response of a spherical cell (rad = 8, $29 \times 29 \times 29$) to a step increase in the uniform applied field. The parameters used in this model solution are shown in Table 1. For these values, the time constant of response for a spherical cell in infinite electrolytes (Eq. (3)) is $\tau_m = 0.33$ μs. A few ns after the step input is applied, U_m is still close to zero. For this time scale, the high frequency response dominates. The dielectric dominated response is demonstrated by the uniform electric field (electrical invisibility of the cell) seen in the corresponding almost parallel equipotentials. In the intermediate time scales ($t \approx \tau_m$, the membrane begins to charge to the asymptotic value (Fig. 4, right). In this temporal region, the field is excluded from the cell following an initial charging phase, as demonstrated by the equipotentials. For longer time scales ($t \gg \tau_m$), U_m reaches a steady state value. The electric field is essentially excluded from the cytoplasm within 2 μs from the application of the step input.

Fig. 4 (right panel) shows the U_m at a pole as a function of time (symmetry dictates that both poles have opposite values). The results show that the response in the transport lattice model is slower than the analytical response. Also, the steady state U_m at the pole of the spherical cell is approximately 10% smaller than the analytical response. The discrepancy can again be attributed to the finite extent of the extracellular medium and the lack of transport along the membrane in the transport lattice model. As in the cylindrical cell case [77], the transport lattice response will approach the analytical response when the system model region is increased beyond the $29 \times 29 \times 29$ used here, which is limited by presently available computer performance.

3.2. Heterogeneous applied field

The spherical cell (rad = 8, $29 \times 29 \times 29$ nodes) is exposed to a heterogeneous electric field created by a planar electrode and a sharp microelectrode (Fig. 5a). The sharp microelectrode, located off-center, is represented by a discretized tetrahedron

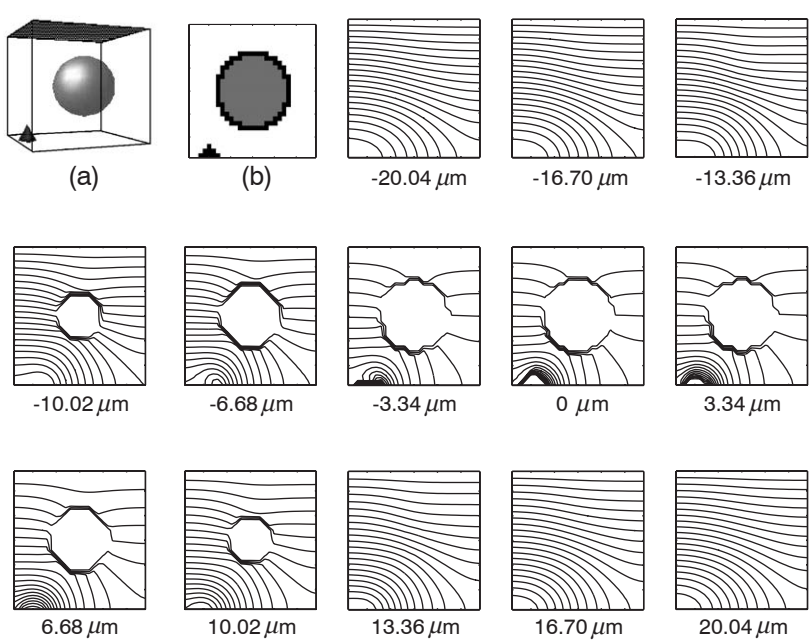

Fig. 5. Equipotentials for a discretized, confined spherical cell between a planar electrode and a sharp microelectrode. (a) Perspective drawing showing the system model cube ($29 \times 29 \times 29$) containing a spherical cell and the electrodes that provide an applied electric field. (b) Approximation of spherical cell (black region assigned M_{e1}; gray region assigned M_{e2} the interface elements assigned $M_{e1+m+e2}$. Equipotentials in selected planes perpendicular to the planar electrode for a 100 Hz applied field. The distance of each plane from the plane through the center of the spherical cell is shown in each panel. The plots show the field excluded from spherical cell because of the high impedance cell membrane. The relative locations of the two electrodes and the cell illustrate our method, but do not seek to maximize U_m at membrane sites nearest the microelectrode.

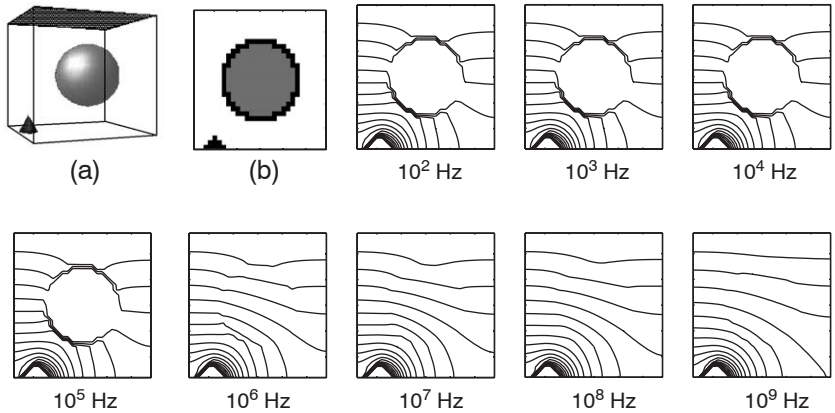

Fig. 6. Frequency response of a discretized, confined spherical cell between a planar electrode and a microelectrode. (a) Perspective drawing showing the system model cube ($29 \times 29 \times 29$) containing a spherical cell and the electrodes that provide an applied electric field. (b) Approximation of spherical cell (black region assigned M_{e1} gray region assigned M_{e2} the interface elements assigned $M_{e1+m+e2}$. Frequency dependence of equipotentials for $f = 100$ Hz to 1 GHz in decades is shown in subsequent panels. The equipotential plots (voltage contours)show the gradual penetration of the response electric field into the spherical cell with increasing frequency for a planar slice through the system model at the center of the sphere.

(Fig. 5b). The heterogeneous electric field in the presence of a spherical cell is seen in the low frequency equipotentials in different planes perpendicular to the planar electrode (Fig. 5) at different distances from the plane through the center of the sphere. As in the uniform electric field case, at low frequencies the electric field is excluded from the cell. Because of the electrode arrangement, even the planes that do not contain the cell also have a heterogeneous electric field. As expected, the electric field is higher in the vicinity of the sharp microelectrode, with or without the cell.

3.2.1. Frequency response

The response electric field distribution in the central plane through the system model region (rad = 8, $29 \times 29 \times 29$ nodes) is shown as equipotentials in Fig. 6. As in the case of spherical cell between parallel plate electrodes [43], the response field changes significantly with frequency. For frequencies less than ~100 kHz, E_{res} is nearly excluded from the cell, while at ~1 MHz the electric field begins to penetrate into the cytoplasm. For 10 to 100 MHz the membrane impedance is negligible, the field inside the cell is larger than that outside the cell because of the larger intracellular resistivity. However, for 1 to 10 GHz, E_{res} is almost uniform throughout the system model, making the cell almost "electrically invisible".

3.2.2. Transient response

As seen in the case of a spherical cell in an uniform electric field, the temporal response is different for different time scales after a step increase in the applied electric field. Fig. 7 shows the response of a spherical cell (rad = 8, $29 \times 29 \times 29$ nodes) to a step increase in the heterogeneous applied field created by a planar electrode and a sharp microelectrode. In addition to the equipotentials, U_m is shown at two locations on the spherical cell: the pole and a point close to the microelectrode.

The heterogeneous electric field penetrates the cytoplasm during the charging phase of the response field ($t \ll \tau_m$). In the intermediate time scales ($t \approx \tau_m$), the membrane begins to charge to the asymptotic value (Fig. 7, right). The field is excluded from the cell following an initial charging phase, as demonstrated by the equipotentials. Within the first 2 μs the

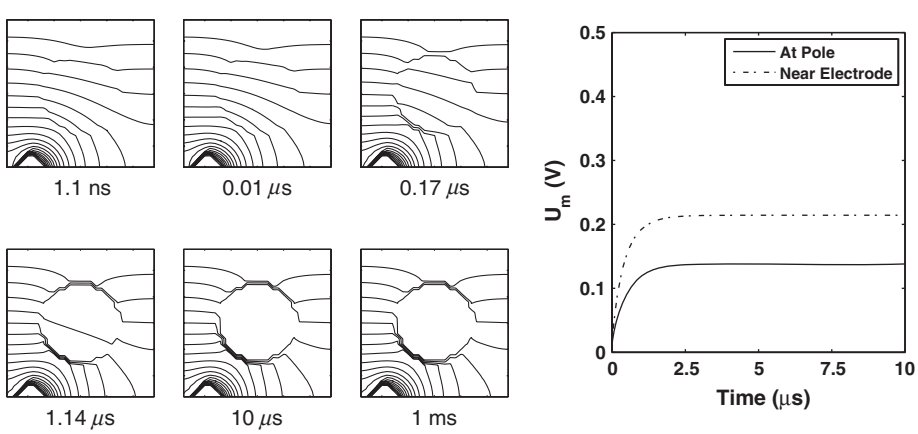

Fig. 7. Step response of a confined spherical cell with a heterogeneous applied field. The equipotentials within a planar slice through the system model at the center of the sphere at different time points are shown in the left panels. The corresponding transmembrane voltage at the pole and at a point near the microelectrode as a function of time is shown on the right side. The applied voltage pulse between the electrodes was increased from 0 to 1 V at $t = 0$. U_m reaches the steady-state value in about 1 μs. Prior to that the response field penetrates the cell because of its high frequency components. In steady-state, the field is excluded from the cell.

field is essentially excluded from the cell. In longer time scales ($t \gg \tau_m$), U_m reaches a steady-state value.

U_m near the electrode in this case of heterogeneous applied field is 0.21 V compared to 0.4 V in the case of uniform applied field created by a 1.0 V pulse across the system model. The definition of pole position is not appropriate for the electrode arrangement in this case. However, for the sake of comparison, we examine U_m at the membrane location that was the pole in the case of uniform applied electric field. We find that U_m at this location is 0.14 V compared to 0.4 V in the case of uniform applied field. The difference is due to the dimension and localized site of the sharp microelectrode which confines much of the voltage drop across the system model to the region near the sharp electrode tip. The small size and offset location of the sharp needle electrode also contributes to the difference in response.

4. Conclusions

With the advancement of micro and nanofabrication techniques, microelectrodes are increasingly being used to locally stimulate and manipulate cells and tissues. Both the applied (E_{app}) and response (E_{res}) electric fields are spatially heterogeneous. Description of such electric fields is not readily accomplished by analytical techniques. In this paper we have demonstrated the use of transport lattice method to study the frequency and time domain response of a spherical cell to homogeneous and heterogeneous applied electric fields. Heterogeneous electric fields are also inevitable in a multicellular system. The transport lattice model approach allows addition of active local models (e.g., resting potential, electroporation) to the system model.

Acknowledgements

We thank G.T. Martin, A. Esser, Z. Vasilkoski, and K.C. Smith for modeling method discussions and K.G. Weaver for computer assistance. Supported by NIH grant RO1-GM63857.

References

[1] C. Polk, E. Postow (Eds.), CRC Handbook of Biological Effects of Electromagnetic Fields, Second Edition, CRC Press, Boca Raton, 1996.
[2] E. Neumann, A.E. Sowers, C.A. Jordan (Eds.), Electroporation and Electrofusion in Cell Biology, Plenum Press, New York, 1989.
[3] D.C. Chang, B.M. Chassy, J.A. Saunders, A.E. Sowers (Eds.), Guide to Electroporation and Electrofusion, Academic Press, New York, 1992.
[4] J.P. Reilly, Electrical Stimulation and Electropathology, Cambridge University Press, Cambridge, 1992.
[5] R.C. Lee, E.G. Cravalho, J.F. Burke (Eds.), Electrical Trauma: The Physiology, Manifestations and Clinical Management, Cambridge University Press, Cambridge, 1992.
[6] D.J. Aidley, The Physiology of Excitable Cells, 4th ed., Cambridge University Press, Cambridge, 1998.
[7] M.J. Jaroszeski, R. Gilbert, R. Heller (Eds.), Electrically Mediated Delivery of Molecules to Cells: Electrochemotherapy, Electrogenetherapy and Transdermal Delivery by Electroporation, Humana Press, Totowa, 2000.
[8] B. Hille, Ionic Channels of Excitable Membranes, Third edition, Sinaur Associates, Sunderland, 2001.
[9] T.E. Vaughan, J.C. Weaver, Molecular change signal-to-noise criteria for interpreting experiments involving exposure of biological systems to weakly interacting electromagnetic fields, Bioelectromagnetics 26 (2005) 305–322.
[10] J.C. Weaver, R.D. Astumian, The response of cells to very weak electric fields: the thermal noise limit, Science 247 (1990) 459–462.
[11] R.D. Astumian, J.C. Weaver, R.K. Adair, Rectification and signal averaging of weak electric fields by biological cells, Proc. Natl. Acad. Sci. 92 (1995) 3740–3743.
[12] J.C. Weaver, T.E. Vaughan, G.T. Martin, Biological effects due to weak electric and magnetic fields: the temperature variation threshold, Biophys. J. 76 (1999) 3026–3030.
[13] T.Y. Tsong, R.D. Astumian, Electroconformational coupling: how membrane-bound ATPase transduces energy from dynamic electric fields, Ann. Rev. Physiol. 50 (1988) 273–290.
[14] B. Robertson, R.D. Astumian, Frequency dependence of catalyzed reactions in an weak oscillating field, J. Chem. Phys. 94 (1991) 7414–7419.
[15] E. Neumann, K. Rosenheck, Permeability changes induced by electric impulses in vesicular membranes, J. Membrane Biol. 10 (1972) 279–290.
[16] M.R. Prausnitz, J.D. Corbett, J.A. Grimm, D.E. Golan, R. Langer, J.C. Weaver, Millescond measurement of transport during and after an electroporation pulse, Biophys. J. 68 (1995) 1864–1870.
[17] P.E. Marszalek, B. Farrell, P. Verdugo, J.M. Fernandez, Kinetics of release of serotonin from isolated secretory granules: I. Amperometric detection of serotonin from electroporated granules, Biophys. J. 73 (1997) 1160–1168.
[18] V. Ganeva, B. Galutzov, E. N., J. Teissié, Electroinduced extraction of β-galactosidase from *Kluyveromyces lactis*, Appl. Microbiol. Biotechnol. 56 (2001) 411–413.
[19] U. Zimmermann, J. Schultz, G. Pilwat, Transcellular ion flow in *Escherichia coli* and electrical sizing of bacterias, Biophys. J. 13 (1973) 1005–1013.
[20] J.K. Kinosita, T.Y. Tsong, Survival of sucrose-loaded erythrocytes in circulation, Nature 272 (1978) 258–260.
[21] E. Neumann, M. Schaefer-Ridder, Y. Wang, P.H. Hofschneider, Gene transfer into mouse lyoma cells by electroporation in high electric fields, EMBO J. 1 (1982) 841–845.
[22] L.M. Mir, H. Banoun, C. Paoletti, Introduction of definite amounts of nonpermeant molecules into living cells after electropermeabilization: direct access to the cytosol, Exp. Cell Res. 175 (1988) 15–25.
[23] D.C. Bartoletti, G.I. Harrison, J.C. Weaver, The number of molecules taken up by electroporated cells: quantitative determination, FEBS Lett. 256 (1989) 4–10.
[24] V.A. Klenchin, S.I. Sukharev, S.M. Serov, L.V. Chernomordik, Y.A. Chizmadzhev, Electrically induced DNA uptake by cells is a fast process involving DNA electrophoresis, Biophys. J. 60 (1991) 804–811.
[25] D.L. Berglund, J.R. Starkey, Introduction of antibody into viable cells using electroporation, Cytometry 12 (1991) 64–67.
[26] M.R. Prausnitz, B.S. Lau, C.D. Milano, S. Conner, R. Langer, J.C. Weaver, A quantitative study of electroporation showing a plateau in net molecular transport, Biophys. J. 65 (1993) 414–422.
[27] R. Heller, M. Jaroszeski, A. Atkin, D. Moradpour, R. Gilbert, J. Wands, C. Nicolau, In vivo gene electroinjection and expression in rat liver, FEBS Lett. 389 (1996) 225–228.
[28] S. Raffy, C. Lazdunski, J. Teissie, Electroinsertion and activation of the C-terminal domain of colicin A, a voltage gated bacterial toxin, into mammalian cell membranes, Mol. Membr. Biol. 21 (2004) 237–246.
[29] M. Zeira, P.-F. Tosi, Y. Mouneimne, J. Lazarte, L. Sneed, D.J. Volsky, C. Nicolau, Full-length CD4 electro-inserted in the erythrocyte membrane as a long-lived inhibitor of infection by human immunodeficiency virus, Proc. Natl. Acad. Sci. 88 (1991) 4409–4413.
[30] F. Hofmann, L.H. Scheller, W. Strupp, U. Zimmermann, C. Jassoy, Electric field pulses can induce apoptosis, J. Membr. Biol. 169 (1999) 103–109.
[31] K.H. Schoenbach, S.J. Beebe, E.S. Buescher, Intracellular effect of ultrashort pulses, Bioelectromagnetics 22 (2001) 440–448.

[32] S.J. Beebe, P.M. Fox, L.J. Rec, K. Somers, R.H. Stark, K.H. Schoenbach, Nanosecond pulsed electric field (nsPEF) effects on cells and tissues: apoptosis induction and tumor growth inhibition, IEEE Trans. Plasma Sci. 30 (2002) 286–292.
[33] E.S. Buescher, K.H. Schoenbach, The effects of submicrosecond, high intensity pulsed electric fields on living cells-intracellular electromanipulation, IEEE Trans. Dielect. Elect. Insul. 10 (2003) 788–794.
[34] P.T. Vernier, Y. Sun, L. Marcu, S. Salemi, C.M. Craft, M.A. Gundersen, Calcium bursts induced by nanosecond electric pulses, Biochem. Biophys. Res. Commun. 310 (2003) 286–295.
[35] P.T. Vernier, L.I. Aimin, L. Marcu, C.M. Craft, M.A. Gundersen, Ultrashort pulsed electric fields induce membrane phospholipid translocation and capase activation: differential sensitivities of Jurkat T lymphoblasts and rat glioma C6 cells, IEEE Trans. Dielect. Elect. Insul. 10 (2003) 795–809.
[36] K.H. Schoenbach, R.P. Joshi, J.R. Kolb, N. Chen, M. Stacey, P.F. Blackmore, E.S. Buescher, S.J. Beebe, Ultrashort electrical pulses open a new gateway into biological cells, Proc. IEEE 92 (2004) 1122–1137.
[37] M. Okino, H. Mohri, Effects of a high-voltage electrical impulse and an anticancer drug on in vivo growing tumors, Jpn. J. Cancer Res. 78 (1987) 1319–1321.
[38] K.T. Powell, A.W. Morgenthaler, J.C. Weaver, Tissue electroporation: observation of reversible electrical breakdown in viable frog skin, Biophys. J. 56 (1989) 1163–1171.
[39] M.R. Prausnitz, V.G. Bose, R. Langer, J.C. Weaver, Electroporation of mammalian skin: a mechanism to enhance transdermal drug delivery, Proc. Natl. Acad. Sci. 90 (1993) 10504–10508.
[40] R.C. Lee, M.S. Kolodney, Electrical injury mechanisms: electrical breakdown of cell membranes, Plast. Reconstr. Surg. 80 (1987) 672–679.
[41] R.C. Lee, D. Zhang, J. Hannig, Biophysical injury mechanisms in electrical shock trauma, Ann. Rev. Biomedical. Eng. 2 (2000) 477–509.
[42] T. Kotnik, D. Miklavcic, Second-order model of membrane electric field induced by alternating external electric fields, IEEE Trans. Biomed. Eng. 47 (2000) 1074–1081.
[43] T.R. Gowrishankar, J.C. Weaver, An approach to electrical modeling of single and multiple cells, Proc. Natl. Acad. Sci. 100 (2003) 3203–3208.
[44] H. Fricke, The electric permittivity of a dilute suspension of membrane-covered ellipsoids, J. Appl. Phys. 24 (1953) 644–646.
[45] H. Pauly, H.P. Schwan, Über die Impedanz einer Suspension von kugelf örmigen Teilchen mit einer Schale, Z. Naturforsch. 14B (1959) 125–131.
[46] J. Gimsa, D. Wachner, Analytical description of the transmembrane voltage induced on arbitrarily oriented ellipsoidal and cylindrical cells, Biophys. J. 81 (2001) 1888–1896.
[47] J. Gimsa, D. Wachner, A polarization model overcoming the geometric restrictions of the Laplace solution for spheroidal cells: obtaining new equations for field-induced forces and transmembrane potential, Biophys. J. 77 (1999) 1316–1326.
[48] L.A. Cartee, R. Plonsey, The transient subthreshold response of spherical and cylindrical cell models to extracellular stimulation, IEEE Trans. Biomed. Eng. 19 (1992) 76–85.
[49] L.M. Livshitz, P.D. Einziger, J. Mizrahi, Rigorous Green's function formulation for transmembrane potential induced along a 3-D infinite cylindrical cell, IEEE Trans. Biomed. Eng. 49 (2002) 1491–1503.
[50] J. Gimsa, D. Wachner, On the analytical description of the transmembrane voltage induced on spheroidal cells with zero membrane conductance, Eur. Biophys. J. 30 (2001) 463–466.
[51] T. Kotnik, R. Bobanovic, D. Miklavčič, Sensitivity of transmembrane voltage induced by applied electric fields—a theoretical analysis, Bioelectrochem. Bioenerget. 43 (1997) 285–291.
[52] T. Kotnik, D. Miklavčič, Theoretical evaluation of the distributed power dissipation in biological cells exposed to electric fields, Bioelectromagnetics 21 (2000) 385–394.
[53] M. Pavlin, D. Miklavčič, Effective conductivity of a suspension of permeabilized cells—a theoretical analysis, Biophys. J. 85 (2003) 719–729.
[54] R. Susil, D. Semrov, D. Miklavcic, Electric field-induced transmembrane potential depends on cell density and organization, Electro-Magnetobiol. 17 (1998) 391–399.
[55] A. Ramos, A. Raizer, J. Marques, A new computational approach for electrical analysis of biological tissues, Bioelectrochemistry 59 (1–2) (2003) 73–84.
[56] C.E. Miller, C.S. Henriquez, Three-dimensional finite element solution for biopotentials: erythrocyte in an applied field, IEEE Trans. Biomed. Eng. 35 (1988) 712–718.
[57] S.M.S. Martin, J.L. Sebastián, M. Sancho, J.M. Miranda, A study of the electric field distribution in erythrocyte and rod shape cells from direct RF exposure, Phys. Med. Biol. 48 (2003) 1649–1659.
[58] T. Heida, J.B.M. Wagenaar, W.L.C. Rutten, E. Marani, Investigating membrane breakdown of neuronal cells exposed to nonuniform electric fields by finite-element modeling and experiments, IEEE Trans. Biomed. Engr. 49 (2002) 1195–1203.
[59] J.R. Buitenweg, W.L.C. Rutten, E. Marani, Extracellular stimulation window explained by a geometry-based model of the nueron-electrode contact, IEEE Trans. Biomed. Eng. 49 (2002) 1591–1599.
[60] D. Panescu, K.P. Cohen, J.G. Webster, R.A. Stratbucker, The mosaic electrical characteristics of the skin, IEEE Trans. Biomed. Eng. 40 (1993) 343–439.
[61] D.B. McGreery, T.G.H. Yuen, W.F. Agnew, L.A. Bullara, A characterization of the effects on neuronal excitability due to prolonged microstimulation with chronically implanted microelectrodes, IEEE Trans. Biomed. Eng. 44 (1997) 931–939.
[62] K.A. Moxon, N.M. Kalkhoran, M. Markert, M.A. Sambito, J.L. McKenzie, J.T. Webster, Nanostructured surface modification of ceramic-based microelectrodes to enhance biocompatibility for a direct brain–machine interface, IEEE Trans. Biomed. Eng. 51 (2004) 881–889.
[63] H.A. Pohl, Dielectrophoresis, Cambridge University Press, London, 1978.
[64] G. Fuhr, W.M. Arnold, R. Hagedorn, T. Muller, W. Benecke, B. Wagner, U. Zimmermann, Levitation, holding, and rotation of cells within traps made by high-frequency fields, Biochim. Biophys. Acta 1108 (1992) 215–223.
[65] T. Heida, W.L.C. Rutten, E. Marni, Dielectrophoretic trapping of dissociated fetal cortical rat neurons, IEEE Trans. Biomed. Eng. 48 (2001) 921–930.
[66] J. Voldman, M.L. Gray, M. Toner, M.A. Schmidt, A microfabrication-based dynamic array cytometer, Anal. Chem. 74 (2002) 3984–3990.
[67] C. Amatore, S. Arbault, D. Bruce, P. de Oliveira, M. Erard, M. Vuillaume, Analysis of individual biochemical events based on artificial synapses using ultramicroelectrodes: cellular oxidative burst, Faraday Discuss. 116 (2000) 319–333.
[68] J.A. Lundqvist, F. Sahlin, M.A. Aberg, A. Stromberg, P.S. Eriksson, O. Orwar, Altering the biochemical state of individual cultured cells and organelles with ultramicroelectrodes, Proc. Natl. Acad. Sci. 95 (1998) 10356–10360.
[69] D.T. Chiu, C.F. Wilson, F. Ryttsen, A. Stromberg, C. Farre, A. Karlsson, S. Nordholm, A. Gaggar, B.P. Modi, A. Moscho, R.A. Garza-Lopez, O. Orwar, R.N. Zare, Chemical transformations in individual ultrasmall biomimetic containers, Science 283 (1999) 1892–1895.
[70] A. Strömberg, F. Ryttsén, D.T. Chiu, M. Davidson, P.S. Eriksson, C.F. Wilson, O. Orwar, R.N. Zare, Manipulating the genetic identity and biochemical surface properties of individual cells with electric-field-induced fusion, Proc. Natl. Acad. Sci. 97 (2000) 7–11.
[71] D.A. Stewart, T.R. Gowrishankar, J.C. Weaver, Transport lattice approach to describing cell electroporation: use of a local asymptotic model, IEEE Trans. Plasma Sci. 32 (2004) 1696–1708.
[72] R.K. Adair, R.D. Astumian, J.C. Weaver, On the detection of weak electric fields by sharks, rays and skates, Chaos 8 (1998) 576–587.
[73] K.A. DeBruin, W. Krassowska, Modeling electroporation in a single cell. I. Effects of field strength and rest potential, Biophys. J. 77 (1999) 1213–1224.
[74] K.A. DeBruin, W. Krassowska, Modeling electroporation in a single cell: II. Effects of ionic concentration, Biophys. J. 77 (1999) 1225–1233.
[75] T.R. Gowrishankar, C. Stewart, J.C. Weaver, Electroporation of a multicellular system: asymptotic model analysis, Proceedings of the 26th

Annual International Conference of the IEEE EMBS, San Francisco, 2004.
[76] T.R. Gowrishankar, D.A. Stewart, G.T. Martin, J.C. Weaver, Transport lattice models of heat transport in skin with spatially heterogeneous, temperature-dependent perfusion, Biomedical. Eng. Online 3 (2004) 42.
[77] D.A. Stewart, T.R. Gowrishankar, K.C. Smith, J.C. Weaver, Cylindrical cell membranes in uniform applied electric fields: validation of a transport lattice method, IEEE Trans. Biomed. Eng. 52 (2005) 1643–1653.
[78] E.C. Fear, M.A. Stuchly, A novel equivalent circuit model for gap-connected cells, Phys. Med. Biol. 43 (1998) 1439–1448.
[79] A. Ramos, D. Suzuki, J. Marques, Numerical simulation of electroporation in spherical cells, Artif. Organs 28 (4) (2004) 357–361.
[80] J.C. Lin, O.P. Gandhi, Computational methods for predicting field intensity, in: C. Polk, E. Postow (Eds.), Handbook of Biological Effects of Electromagnetic Fields, 2nd Edition, CRC Press, Boca Raton, 1996, pp. 337–402.
[81] J. Hilland, Simple sensor system for measuring the dielectric properties of saline solutions, Meas. Sci. Technol. 8 (1997) 901–910.
[82] D.C. Mikulecky, Applications of Network Thermodynamics to Problems in Biomedical Engineering, New York University Press, New York, 1993.
[83] A. Vladimirescu, The SPICE Book, John Wiley and Sons, New York, 1994.
[84] J.C. Neu, W. Krassowska, Asymptotic model of electroporation, Phys. Rev., E 59 (1999) 3471–3482.
[85] J.C. Neu, K.C. Smith, W. Krassowska, Electrical energy required to form large conducting pores, Bioelectrochemistry 60 (2003) 107–114.
[86] K.C. Smith, J.C. Neu, W. Krassowska, Model of creation and evolution of stable electropores for DNA delivery, Biophys. J. 86 (2004) 2813–2826.
[87] S.A. Freeman, M.A. Wang, J.C. Weaver, Theory of electroporation for a planar bilayer membrane: predictions of the fractional aqueous area, change in capacitance and pore–pore separation, Biophys. J. 67 (1994) 42–56.
[88] C. Mudd, Evaluation of phase transition errors in heat capacity calorimeters using SPICE simulated RC models, J. Biochem. Biophys. Methods 39 (1999) 7–38.